Effects of Driving Style on Energy Consumption and CO$_2$ Emissions

Susana Carreón-Sierra[1] · **Alejandro Salcido[2]**

[1] Maestría en Ciencias de la Complejidad, Universidad Autónoma de la Ciudad de México, Mexico City, Mexico,
E-mail: scarreons@gmail.com

[2] Departamento de Física, Universidad Autónoma Metropolitana, Iztapalapa, Mexico City, Mexico,
E-mail: vasalcido@xanum.uam.mx

Abstract The tractive force developed by energy consumption (EC) in a car engine produces its acceleration and sustains the motion against velocity dependent resistance forces. In internal combustion engines, fuel burning entails pollutant emissions (PE) released into the atmosphere. In vehicular traffic, EC and PE depend on the driving style. This paper assumed that the transition rules in a traffic cellular automata (TCA) represent a driving style, and its effect on EC and PE in TCA is studied. Extending empirical relationships, we proposed models to estimate EC and PE in TCA from the velocity and acceleration distributions, which we obtained by computer simulations for three well-known TCA. The Nagel-Schreckenberg (NS) and Fukui-Ishibashi (FI) models, and a variant (NS+FI) defined by combining the NS and FI rules, were considered. The FI driving style revealed EC and CO$_2$ emission rates dependent on the stochastic delay (p) only for low vehicular densities. We also detected that the larger EC and CO$_2$ emission rates were $45.4 kW$ and $26.7 g/s$ with no dependence on p. With NS and NS+FI driving styles, the larger energy consumption and CO$_2$ emission rates occurred for small stochastic delays, $18.4 kW$ and $6.6 g/s$ and $61.1 kW$ and $30.2 g/s$ for $p = 0.2$. On average, for NS, FI, and NS+FI models ($p = 0.2$), we obtained energy consumptions of 1.88, 2.60, and $2.76 MJ/km$, fuel consumptions of 0.08, 0.12, and $0.13 L/km$, and CO$_2$ emissions of 0.158, 0.460, and $0.562 kgCO_2/km$. Our results agree with those ($3.37 MJ/km$ and $0.235 kgCO_2/km$) of petrol combustion car engines at $10 km/L$. This work may help in designing flow and driving style scenarios to optimize vehicular traffic EC and reduce PE.

Keywords Energy consumption · CO$_2$ emissions · velocity and acceleration distribution · cellular automata model

1 Introduction

Vehicular traffic congestion is a severe problem worldwide, which causes substantial economic loss, large energy consumption, and atmospheric pollution. For more than four decades, traffic flow studies have attracted the interests of scientists from various disciplines. The scientific treatment of the traffic flow phenomena began with Robert Herman in 1956 [1], and some years later, Herman and Prigogine started to study vehicular traffic as a collective flow phenomenon, developing a kinetic theory for multi-lane traffic flow using a Boltzmann like model for the vehicle interactions [2]. In the second half of the 1980s, a new line of research emerged for traffic flow simulation based on cellular automata [3], although its proper development started in the early 1990s with the models proposed by K. Nagel and M. Schreckenberg [4] and by M. Fukui and Y. Ishibashi [5], hereafter referred as the NS and FI models. Several excellent and complimentary reviews of the different traffic flow approaches have been published. In 2000, D. Chowdhury, L. Santen, and A. Schadschneider [6] wrote a critical review of microscopic models of vehicular traffic from the perspective of statistical physics. They explained the guiding principles behind all the main theoretical approaches, and presented detailed discussions on the results obtained mainly from the particle-hopping models, emphasizing those formulated using cellular automata techniques. D. Helbing [7], in 2001, reviewed the main approaches to modeling pedestrian and vehicle traffic considering the empirical data. He pointed out that fuel consumption would increase by 2–4 times when vehicle velocity increases from 10 to 40 km/h which would lead to the same multiple increase of CO_2 emission. The Helbing's review included microscopic (particle-based), mesoscopic (gas-kinetic), and macroscopic (fluid dynamic) models, paying attention to the formulation of a micro-macro link, to aspects of universality, and to other unifying concepts, such as a general modeling framework for self-driven many-particle systems. One year later, T. Nagatani [8] published an overview of traffic physics, where attention was paid to the formulation of the traffic dynamics, the dynamical phase transitions and the nonlinear waves. Nagatani discussed the methods and results for the car-following models in detail after explaining the traffic models and the micro–macro link. He focused on the dynamical phase transitions and the nonlinear density waves from the point of view of statistical physics and nonlinear waves. In addition, he described the linear stability theory in detail to explain the jamming transitions. In 2003, K. Nagel, P. Wagner, and R. Woesler [9] published an outstanding paper where they look at intuitive and formal arguments regarding traffic jams, including their formation and their stability, providing also an overview of empirical facts. They look at microscopic models for traffic, including coupled differential equation models, cellular automata models, and coupled maps. These studies help to understand the traffic flow dynamics and may contribute to implement strategies to mitigate traffic congestion. Traffic flow also involves a self-driven many-particle system far from equilibrium, where the nonlinear interactions among vehicles give rise to exciting phenomena, such as boundary-induced phase transitions, spontaneous jams, and metastability, hysteresis, and phase-separation [10–12]. Therefore, traffic flow studies also contribute to investigating fundamental aspects of nonequilibrium systems of interest in complexity sciences [13].

Vehicle energy consumption and engine emissions are two critical aspects considered in the transportation planning process of highways and road facilities. Transportation is one significant contributor to human-made polluting emissions. Individually, the pollutant emissions from cars are generally low. However, since the number of motor vehicles in urban settlements is enormous, the combined emissions and energy consumption cannot be disregarded. The pollutant emissions from vehicular traffic driven by fossil fuel combustion depend on fuel chemical composition and consumption, so as the quality of the combustion process. Therefore, we need the vehicle characteristics, traffic circumstances, and road conditions to estimate the expected energy consumption and the associated vehicular pollutant emissions.

According to Newtonian mechanics, the net force exerted on a vehicle in the direction of motion is proportional to its acceleration once this force overcomes the friction forces, such as the aerodynamic and rolling resistances. Tractive effort and resistance are the principal forces opposing each other, which decide roadway vehicle performance. Tractive force is exerted against the roadway surface, allowing the vehicle motion. Resistance comprises all the forces that push back and impedes motion. Then,

$$F_T(v,a) = ma + F_R(v) \tag{1}$$

Here, m and a are the vehicle's mass and acceleration, and F_R denotes the friction forces.

The main friction forces are the aerodynamic, rolling, and grade resistances. There are simple models for estimating the first two resistances from the speed and some other attributes, such as mass and frontal area of the vehicle and the road characteristics [14–16]. The grade resistance is conceptually simple and depends on the slope of the road, but its determination is complicated because of the road surface variability [17]. In this work, we will not consider the influence of grade resistance on vehicle power and fuel consumption.

Eq. 1 highlights the importance of knowing the vehicles' spatial and temporal distributions of velocity and acceleration for assessing the fuel (energy) consumption and the associated pollutant emissions under the different traffic conditions and driving styles. It also underlines the need of developing and applying theoretical and experimental strategies to determine these distributions.

From the experimental standpoint, although there are vast amounts of empirical data collected by loop detectors, video cameras, and floating cars, we are still not able to know exactly how the traffic flow evolves even in simple scenarios, such as in a platoon of cars following each other without overtaking and led by a car moving with constant velocity [13]. Moreover, the empirical observations are site-specific and involve confounding factors, such as geometry, bottleneck strength, and traffic flow composition, which forestall us from obtaining a comprehensive understanding of traffic flow behavior. Traffic flow modeling could be an essential step in the design and control of transportation systems and help to accurately and realistically predict traffic flow; however, no complete and comprehensive model exists to capture the richness and complexity of real traffic.

In the last two decades, the cellular automata models for traffic flow (or traffic cellular-automata (TCA)) emerged as an up-and-coming alternative to existing traffic flow models

[4, 5, 9, 12, 18–22]. In contrast with existing models, which are either aggregate in their treatment of traffic flow (macroscopic models) or detailed and limited in scope (microscopic models), the TCA involve the individual vehicle interactions and dynamics and relate them to macroscopic traffic flow attributes, such as throughput, travel time, and vehicle speed. These models can encapsulate the complexity of real-world traffic behavior, producing clear physical patterns similar to those we see in everyday life. These models can more adequately capture the complexity of real traffic by allowing different vehicles to possess different driving behaviors (acceleration/deceleration, lane change rules, and reaction times).

Numerous works have reported many interesting results on energy consumption and pollutant emission of vehicular traffic from different modelling standpoints, such as the car-following and cellular automata traffic approaches. Toledo et al. [23] introduced a microscopic traffic model, based on kinematic behaviour, which consists of a single vehicle traveling through a sequence of traffic lights that turn on and off with a specific frequency. They showed that the traffic variables such as travel time, velocity, and fuel consumption follow critical scaling laws near a resonance, suggesting the existence of a universal behaviour of the system in the vicinity of the resonant condition. Shi and Xue [24], studied the relation between the energy consumption and the stability of vehicle flow in several car-following traffic models including the cooperative driving with weight factors and relative velocity. They showed that for more stable traffic flow, the less energy consumption becomes less. These results can help to choose the optimal traffic model with lower energy consumption to reduce air pollution. Zhang et al. [25] studied energy dissipation rate in deterministic and non-deterministic NS models. They obtained the relationships between the energy dissipation with the speed limit, the stochastic noise, the boundary conditions and the "go and stop" traffic. Zhu [26] investigated the CO_2 emission rate in traffic flow from the analytical and numerical standpoints. They used an emission model derived from the Bando's optimal velocity model with a consideration of slope. Simulations were conducted to examine the relationship between the CO_2 emission rate of vehicles and slope of road, traffic density, and road length. The results showed that some original laws of CO_2 emission in traffic flow with congestion were exhibited. Tang et al. (2013) [27] used a car-following model to study the vehicle's fuel consumption with consideration of the traffic interruption probability under two traffic situations. The numerical results show that the car-following model with consideration of traffic interruption probability can reduce vehicle's fuel consumption in the studied traffic situations and thus improve the vehicle's fuel economy. Tang et al. (2014) [28] used empirical data to calibrate the speed-headway function and proposed a car-following model to investigate the effects of real-time road condition on each vehicle's speed, acceleration, headway, fuel consumption, and emissions of CO, HC and NOX under uniform flow. Their results showed that real-time road condition produces oscillating phenomena and enhance each vehicle's fuel consumption and exhaust emissions. Xue et al. (2014) [29] proposed a cellular automaton traffic model to investigate the energy dissipation in an on-ramp traffic system. They considered the traffic behavior in on-ramp flow system and the variation of energy dissipation in it. The influences of the injected probabilities and removed probability on energy dissipation were studied numericaly. The results showed the existence

of a critical point for the injected probability and a platform for energy dissipation, and indicated that the removed probability plays a relevant role in avoiding traffic jam and reducing the energy dissipation and the vehicle emission. Tang et al. (2015) [30] used the car-following model to explore the impacts of on-ramp on the vehicle's fuel consumption on the main road under uniform flow. Their numerical simulations showed that on-ramp can enhance each vehicle's fuel consumption on the main road and that the increments are related to the traffic state of the main road and the inflow of the on-ramp. On another work, Tang et al. (2017) [31], used their model to investigate the effects of a signal light on the vehicle's fuel consumption and HC, CO and NOx emissions on a road with open boundary condition. They showed that the effects are related to the green split of the signal light and the vehicle's time headway at the origin. Jin et al. [32] proposed a modified car-following model that takes into account the influence of the average speed effect of vehicles and driver's memory on traffic flow basing on two velocity difference model. The time-dependent Ginzburg–Landau equation and the modified Korteweg–de Vries equation were constructed to describe the traffic behaviour near the critical point. The evolution of traffic congestion and the corresponding energy consumption are discussed. Ma et al. [33] proposed improvements to the car-following and the Virginia Tech microscopic (VT-Micro [14]) models to study the impact of the acceleration with memory on stabilization of traffic flow and vehicle's fuel consumption. Numerical results showed that the effect of acceleration with memory can gradually dissipate traffic congestion and reduce energy consumption. Xue et al.(2020) [34] studied the energy consumption of vehicles on one-way lanes under open boundary conditions with the Kerner-Klenov-Wolf three-phase cellular automaton traffic model. Numerical simulations for energy consumption on free flow, congested phase, synchronous flow, and maximum current indicate that the injection and removal rates significantly impact energy consumption in the open boundary traffic system. Qiao et al. [35] investigated the particulate matter emission of two cellular automata traffic models with slow-to-start rule (VDR [10] and TT [36] models) by combining an empirical particulate emission model (proposed by Int Panis et al. [37]) under periodic boundary and open boundary conditions. Lakouari et al. [38] used the cellular automaton NS model combined with the emission model [37] to simulate the CO$_2$ emission at the roundabout. Binoua et al.[39] used the NS model to investigate the dependence of the CO$_2$ emission on the traffic lights. They considered the difference between the two types of traffic lights control, the synchronized traffic lights and green wave controls.

In the simplest case of the single-lane traffic flow, the cellular automata models share the following properties [19]: indistinguishable particles with unitary mass represent the vehicles, they move in a 1D lattice gas obeying an exclusion principle (no more than one particle in one lattice site), the particle velocity is a non-negative integer that cannot exceed a given limit, the dynamic rules prevent collisions and overtaking, and are applied to all particles simultaneously, the number of particles is a conserved property. It is important to stress that the dynamical rules of the TCA are not microscopically reversible in general (do not satisfy the principle of detailed balance [40]) and, therefore, define out-of-equilibrium systems. No complete theory exists for TCA, except for some particular models [19]. Therefore, in general, even with the simplest single-lane traffic flow models proposed by Nagel and Schreckenberg (NS) [4, 18] and Fukui and Ishibashi (FI) [5, 12],

one studies the TCA behavior through computer simulations.

In this paper, we used the TCA models to study the steady-state velocity and acceleration distributions of single-lane traffic by computer simulations, and also for estimating the associated energy consumption and CO_2 emissions. We carried out the simulations under periodic boundary conditions and determined the velocity and acceleration distributions under (virtually) steady-state conditions for several values of the particle density and stochastic delay (the main control parameters of the system). Then, we estimated the energy consumption rate from the tractive force power, which we determined using resistance force simple models reported in the literature [15, 16, 41]. To estimate the CO_2 emissions of the simulated vehicular traffic, we used the velocity and acceleration distributions and an extension of an empirical model proposed by Int Panis et al.[37]. For comparison purposes, we used the EPA emission factor [42] to estimate de CO_2 emissions of a petrol combustion engine.

Although one can find simple empirical models to estimate the vehicular pollutant emission rate from emission factors depending on the vehicle velocity only [43, 44], the more representative theoretical or empirical vehicular energy consumption and pollutant emissions models require the velocity and acceleration distributions as the primary inputs. This paper presented, up to our knowledge, the first estimations of steady-state velocity and acceleration distributions for TCA models and their application to estimate their energy consumption and CO_2 emissions.

2 Methods

Cellular automata (CA) constitute a class of spatially and temporally discrete dynamical systems characterized by local interactions and synchronous evolution [45]. They are prototypes for complex systems and processes comprised of many simple, homogeneous, locally interacting components. Cellular automata can generate a rich spectrum of very intricate behavior patterns based on relatively simple subjacent rules [45, 46], and they appear to capture many essential features of complex self-organizing cooperative behavior observed in natural systems [46].

The physical environment of a cellular automaton is a finite-dimensional lattice, where each site has a finite number of discrete states. The states of the lattice sites define the state of the complete system. It evolves in discrete time steps following a given transition rule, which can be deterministic or probabilistic. Frequently, the transition rule has some simplifying features: it is homogeneous (all sites evolve according to the same rule), but one could also consider inhomogeneous cellular automata; it is spatially local (the transition rule depends only on the states of the sites in a given local neighborhood of the site of interest); it is synchronic (all lattice sites are updated simultaneously); it is temporally local (the rule depends only on the site states at very few previous time-steps).[45, 46]

2.1 Traffic Cellular Automata

The application of CA to the traffic flow problems goes back to Cremer and Ludwig [47], Nagel and Schreckenberg [4], and Fukui and Ishibashi [5]. The development of TCA stimulated the research activity to understand and control traffic instabilities responsible for stop-and-go traffic and congestion on freeways and urban streets [6, 48]. Nowadays, cellular automata are popular frameworks for the microscopic simulation of traffic flow, including multilane highways and complex urban traffic networks. However, no reports exist about the steady-state distributions of velocity and acceleration in TCA and their application to estimate energy consumption and pollutant emissions. This paper used the NS and FI models, and a variant combining them, to study vehicular traffic velocity and acceleration distributions under steady-state conditions and their associated energy consumption and CO$_2$ emission.

2.1.1 The Nagel and Schreckenberg Model

In the NS model [4, 18], space and time are discrete and hence, also the velocities. The road is modeled by a 1D lattice with a number L (finite or infinite) of sites representing vehicle positions. In general, we defined the time step δt and the distance between adjacent lattice sites δs as a unit in CA models; however, for comparison with real traffic, it is usual to define δt as one second and δs as the front-bumper-to-front-bumper average distance of cars under jamming conditions and taken equal to 7.5m [7]. Each site of the lattice is empty or occupied by one vehicle that can be at rest ($v = 0$) or moving left to the right along the lattice with an integer speed $v = 1, 2, 3, \ldots, v_{max}$. The following rules define the time evolution of the system. These rules act on all vehicles (i.e., on all the non-empty lattice sites) simultaneously. If at time t, there is a vehicle at site c ($c = 1, 2, 3, ..., L$), moving with velocity $v(c,t)$, and with a number $h(c,t)$ of empty sites in front of the vehicle, then the velocity updating is performed in two steps. Step 1 (acceleration/braking): $v(c,t) \rightarrow u(c,t) = min\{v(c,t) + 1, h(c,t), v_{max}\}$; the vehicle speed is at most increased by 1 at each time-step. Step 2 (randomization): with probability p, $v(c,t+1) = max\{u(c,t) - 1, 0\}$, but with probability $1 - p$, $v(c,t+1) = u(c,t)$. Finally, the car moves from site c to site $c + v(c,t+1)$. Parameter p is called stochastic delay.

2.1.2 The Fukui-Ishibashi Model

In the FI model [5, 12], the vehicles can move by at most a number v_{max} of lattice sites in one time-step if vehicles in front do not block them. In detail, if at time t, the number of empty sites h in front of a car is larger than v_{max}, then this particle can move forward v_{max} (or $v_{max} - 1$) sites in the next time-step with probability $1 - p$ (or p). If $h < v_{max}$ at time t, then the car can only move by h sites in the next time. Here, the probability p represents the degree of stochastic delay. No driver would like to slow down when far away from the vehicle ahead. In the high-density case, the stochastic delay represents the assurance of the avoidance of crashes. The FI model differs from the NS model in that the increase in speed may not be gradual and that stochastic delay only applies to the fast vehicles. The

FI model can be considered as a NS model with *aggressive driving style*, since at each step every car can accelerate to v_{max} (or $v_{max} - 1$, depending on p).

2.1.3 The NS + FI Model

In 2007, Chuan-Ji Fu et al. [49] introduced a new TCA which consists of a modified Nagel–Schreckenberg model with the Fukui–Ishibashi acceleration rule. In this model, it is adopted the acceleration rule introduced by Fukui and Ishibashi, but modified for the stochastic delay is also applied to slow vehicles. If at time t, there is a vehicle at site c ($c = 1, 2, 3, ..., L$), moving with velocity $v(c,t)$ with a number $h(c,t)$ of empty sites in front of it, then the velocity updating is performed as follows

$$v(c,t+1) = \begin{cases} 0 & \text{if } h(c,t) = 0 \\ h(c,t) - 1 & \text{with probability } p, \text{ if } 0 < h(c,t) < v_{max} \\ h(c,t) & \text{with probability } 1 - p, \text{ if } 0 < h(c,t) < v_{max} \\ v_{max} - 1 & \text{with probability } p, \text{ if } h(c,t) \geq v_{max} \\ v_{max} & \text{with probability } 1 - p, \text{ if } h(c,t) \geq v_{max} \end{cases}$$

2.2 Velocity and Acceleration Distributions

In general, we can describe the state of a 1D TCA with the number of lattice cells (L) and the numbers N_i of the vehicles that are moving with each one of the allowed velocities $v_i = i$ ($i = 0, 1, 2, \ldots, v_{max}$) [19]. Conveniently, we can use intensive properties, such as the partial densities defined as

$$n_i = \frac{N_i}{L} \tag{2}$$

The numbers n_i define the velocity distribution of the selected traffic model; they specify the number of vehicles per site that move with velocity v_i.

The vehicular density n is equal to the sum of all the partial densities n_i

$$n = \sum_{i=0}^{v_{max}} n_i \tag{3}$$

and the number of cars in the lattice is $N = nL$.

The traffic flow (or density of momentum) q and the density of kinetic energy ε are given by

$$q = n\bar{v} = \sum_{i=0}^{v_{max}} v_i n_i \tag{4}$$

$$\varepsilon = \sum_{i=0}^{v_{max}} \varepsilon_i n_i \tag{5}$$

where $\varepsilon_i = v_i^2/2$ is the kinetic energy of a car moving with speed v_i. We observe that $\bar{v} = q/n$ is the average speed of the traffic flow. In general, the partial densities n_i will be functions of the density n and the stochastic delay p.

Depending on the model dynamics, each car can increase or decrease its velocity between 0 and v_{max}. If at time t, in a cell c is located a car moving with a velocity $u(c,t)$, the rules of the model will change this velocity to $u(c,t+1)$,

$$u(c,t+1) = \mathscr{D}(u(c,t),h(c,t),p,v_{max}) \tag{6}$$

Here, $\mathscr{D}$ denotes the set of rules that define the model dynamics. These rules, in general, are defined in terms of the velocity $u(c,t)$ of the car at the cell of interest at time t, the distance $h(c,t)$ (number of free cells) to the next car ahead at time t, a random braking probability (or stochastic delay) p, and the speed limit v_{max}.

The acceleration $a(c,t)$ of the car is the velocity change per unit time given by

$$a(c,t) = u(c,t+1) - u(c,t) = \mathscr{D}(u(c,t),h(c,t),p,v_{max}) - u(c,t) \tag{7}$$

In principle, the acceleration $a(c,t)$ can assume values $a_j = j$ with

$$j = -v_{max}, \ldots, -1, 0, 1, \ldots, v_{max}, \tag{8}$$

although it will depend on the value of $u(c,t)$. We will describe the acceleration distribution in terms of a $(v_{max} + 1) \times (2v_{max} + 1)$ matrix $\mathbf{A}$. The element A_{ij} gives the fraction of cars in the system with velocity v_i and acceleration a_j. Under steady-state conditions, the functions A_{ij} will only depend on the particle density and stochastic delay.

2.3 Estimation of Energy Consumption

The calorific value of a fuel is the amount of energy (heat) released during the combustion of the unit of mass of fuel (expressed as $kcal/kg$ or $Joule/kg$). On average, the calorific value for gasoline is $45MJ/kg$. Then, if Q and Q_0 are the instantaneous and idle fuel consumption rates of a fossil fuel combustion vehicle, the difference $Q - Q_0$ is proportional to the instantaneous vehicle power, $P = vF_T(v,a)$,

$$Q(v,a) - Q_0 = kP(v,a) = kvF_T(v,a) \tag{9}$$

where k is a constant, and v and a are the vehicle's speed and acceleration. The value of k depends on the fuel's chemical composition and thermodynamic properties, and Q_0 depends on the engine characteristics and the quality of the internal combustion process.

Using Eq. 1, we can write

$$Q(v,a) - Q_0 = kv\left[ma + F_R(v)\right] \tag{10}$$

For TCA with identical model vehicles, the vehicle power,

$$P(v,a) = \frac{Q(v,a) - Q_0}{k} = v\left[ma + F_R(v)\right] \tag{11}$$

constitutes an appropriate measure of the energy consumption rate.

Eq. 11 gives the required power as a function of velocity and acceleration in all driving situations where acceleration has a non-negative value. For negative acceleration, corresponding to braking or downhill situations, the fuel consumption depends on the motor management and the driving style. In this work, we assume flat terrain highways (no downhill situations), and the negative accelerations will be associated with braking without using the motor brake. Additionally, we will not consider hybrid cars, where kinetic energy charges the batteries. Moreover, Eq. 11 does not considers the energy consumption by the engine of a stopped vehicle. Under engine idle conditions, energy is consumed only if the car is in motion.

To estimate the energy consumption of a traffic cellular-automata, we propose the following extension of Eq. 11 for any lattice cell c and time t,

$$P(c,t) = \sum_{i=0}^{v_{max}} \left\{ F_R(v_i)v_i n_i(c,t) + \sum_{j=-v_{max}}^{v_{max}} (mv_i a_j)A_{ij}(c,t) \right\} \qquad (12)$$

2.4 The Resistance Forces

There are simple models for the aerodynamic and rolling resistance forces. Following [15, 16, 41, 50], we will use the formulas described below.

2.4.1 Aerodynamic Resistance

The turbulent airflow around the vehicle body produces aerodynamic resistance. This turbulence depends on the vehicle shape and the friction of air passing over the vehicle surface. A small contribution to this resistance comes from airflow through vehicle components, such as interior ventilation. A simple model to estimate the aerodynamic resistance [50] is:

$$R_A = \frac{\rho A C_D v^2}{2} \qquad (13)$$

Here, ρ is the air mass density, A is the vehicle's frontal area, C_D is the drag coefficient, and v is the vehicle's speed. The frontal area and drag coefficient are generally unique to each vehicle or type of vehicle.

2.4.2 Rolling Resistance

The interaction of the vehicle tires with the roadway surface produces the rolling resistance. The leading causes of rolling resistance are the tire rigidity and the roadway surface, the tire pressure and temperature, the vehicular operating speed, and vehicle weight (mg). The value of rolling resistance is given by the simplified formula [50],

$$R_R = (\mu_0 + \mu_1 v)mg \qquad (14)$$

Parameter	Symbol	Value
Vehicle mass	m	$1600kg$
Friction coefficient	μ_0	0.015
Friction coefficient	μ_1	$0.0003s/m$
Cross-sectional-area	A	$2.03m^2$
Air drag coefficient	C_D	0.32

Table 1   Car data for typical passenger cars [50].

2.4.3 Energy Consumption Rate in TCA

Using the expresions for the aerodynamic and rolling resistances, Eq. 12 becomes to

$$P(c,t) = \sum_{i=0}^{v_{max}} \left\{ \left[\frac{\rho A C_D v_i^2}{2} + (\mu_0 + \mu_1 v_i)mg \right] v_i n_i(c,t) + \sum_{j=-v_{max}}^{v_{max}} (m v_i a_j) A_{ij}(c,t) \right\} \quad (15)$$

This equation describes the energy consumption rate per site of the vehicles moving with velocities and accelerations distributed according to n_i and A_{ij}. Under steady-state conditions, the distributions of velocity and acceleration, n_i and A_{ij}, depend only on the particle density n and the stochastic delay p, and Eq. 15 gives the vehicular power per site of the system $P(n,p)$. This equation involves some parameters specific for the vehicle type. In Tab. 1, we presented some typical values for passenger cars as reported in [50].

Although generally defined as a unit, the distance among adjacent cells in the lattice is assumed to be the average front-bumper-to-front-bumper distance of adjacent vehicles under conditions of strongly jammed traffic and set for real traffic simulations to $7.5m$ [7]. If the time step is set equal to one second, the vehicle velocity will change in steps of $27km/h$. Therefore, when comparing with actual traffic data, the interpretations of the model velocities are

$$v_0 = 0, v_1 = 27, v_2 = 54, v_3 = 81, v_4 = 108, v_5 = 135km/h \quad (16)$$

2.5 Estimation of CO$_2$ Vehicular Emissions

We considered the carbon dioxide emission because of its adverse effects on the global heating phenomenon and its direct link with fuel consumption (according to the US-EPA emission factors [42], $2.35kg$ of CO$_2$ are released to the atmosphere each liter of fuel combusted, on average). We estimated the CO$_2$ emissions for TCA models using an empirical model proposed in 2006 by Luc Int Panis, Steven Broekx, and Ronghui Liu [37]. This emission model (hereafter referred to as PBL model) is based on empirical measurements that relate vehicle emissions to engine type and instantaneous speed and acceleration.

Because of its simplicity, many researchers have adopted the PBL model to study vehicular emissions. Moreover, the PBL model can predict the urban traffic emission of

Engine Type	f_0	f_1	f_2	f_3	f_4	f_5
Gasoline	0.553	0.161	-0.00289	0.266	0.511	0.183
Diesel	0.324	0.0859	0.00496	-0.0586	0.448	0.230
LP gas	0.600	0.219	-0.00774	0.357	0.514	0.170

Table 2 Constants for the CO_2 emission function for urban traffic [37].

CO_2 within the 95% confidence interval, using only the vehicles acceleration and speed as predictors [37, 38, 51]. Nyhan et al. [51] used data routinely captured by existing transportation networks and vehicle fleets to predict vehicular emissions in high spatial resolution. They implemented a microscopic emissions model based on the PBL model to predict CO_2, NO_x, VOC, and PM emissions throughout the study domain. Pan et al. [52] combined the classical NS traffic model and the empirical emission function of the PBL model to investigate the effects of traffic congestion on the atmosphere due to the emitted particulate matter from on-the-road vehicles, and also the impact on the fuel rate and dissipation. Astarita et al. [53] estimated the energy and air quality impacts of a single intersection signal regulation by evaluating fuel consumption and pollutant emissions, demonstrating that significant improvements in air quality are possible by introducing floating car data regulated traffic signals. Madani and Moussa [54] adopted cellular automaton to simulate fuel consumption and engine pollutant using a simple emission model that resembles the emission factor approach. Wang et al. [55] studied pollutant emissions of mixed traffic flow with a cellular automaton traffic model based on the NS model, coupled with an empirical emission procedure derived from the PBL model. In the PBL model, using nonlinear multiple regression, a general function for all pollutant emissions was derived for each vehicle type with instantaneous speed and acceleration as parameters. The emission rate of a given vehicle moving with speed $v(t)$ and acceleration $a(t)$ at time t is estimated as

$$G(v,a) = f_0 + f_1 v(t) + f_2 v(t)^2 + f_3 a(t) + f_4 a(t)^2 + f_5 v(t)a(t) \qquad (17)$$

Here, f_k ($k = 0, 1, \ldots 5$) are constants specific for each pollutant and type of vehicle engine. Int Panis et al. [37] reported these constants for CO_2, NO_x, COV, and PM for gasoline, diesel, and LP gas engines. Tab. 2 presents the constants for CO_2 emissions and gasoline, diesel, and LP gas engines. The emission rate unit is g/s if the speed and acceleration are expressed in m/s and m/s^2, respectively.

2.5.1 CO_2 Emission Rates in TCA

To estimate the CO_2 emission rate per site of a traffic cellular-automata, we propose the following extension of Eq. 17 for any lattice cell c and time t,

$$G(c,t) = f_0 n_0 + \sum_{i=0}^{v_{max}} \left\{ \left[f_1 v_i + f_2 v_i^2 \right] n_i + \sum_{j=-v_{max}}^{v_{max}} \left[(f_3 a_j + f_4 a_j^2) + f_5 v_i a_j \right] A_{ij} \right\} \qquad (18)$$

where $n_i = n_i(c,t)$ and $A_{ij} = A_{ij}(c,t)$, and the constants $f_0, \ldots, f_5$ as given in Tab. 2.

Under steady-state conditions, the distributions of velocity and acceleration, n_i and A_{ij}, depend only on the particle density n and the stochastic delay p of the system. For any couple (n,p), $n_i(n,p)$ gives the fraction of vehicles moving in the system with the velocity v_i, and $A_{ij}(n,p)$ gives the fraction of vehicles in the system with velocity v_i and acceleration a_j. This case, Eq. 18 gives the CO$_2$ emission rate per site of a TCA as $G(n,p)$.

Eq. 18 gives the CO$_2$ emission rate per lattice-site as a function of velocity and acceleration distributions in all driving situations where acceleration has a non-negative value. For negative acceleration, corresponding to braking or downhill situations, the fuel consumption and emissions depend on motor management style. We will assume no downhill situations, and the negative accelerations will be associated with mechanical braking (i.e., without using the engine brake). Eq. 18 comprises four contributions, which, for future reference, we will denote as

$$C(0) = f_0 n_0 \tag{19}$$

$$C(v) = \sum_{i=0}^{v_{max}} \left(f_1 v_i + f_2 v_i^2 \right) n_i \tag{20}$$

$$C(a) = \sum_{i=0}^{v_{max}} \sum_{j=-v_{max}}^{v_{max}} \left(f_3 a_j + f_4 a_j^2 \right) A_{ij} \tag{21}$$

$$C(va) = \sum_{i=0}^{v_{max}} \sum_{j=-v_{max}}^{v_{max}} f_5 v_i a_j A_{ij} \tag{22}$$

The term $C(0)$ is the contribution of the vehicles stopped to the emission rate, $C(v)$ gives the contribution of the vehicles moving with the velocities $v_1, v_2, \ldots v_{max}$, $C(a)$ is the contribution of the vehicles moving with velocity v_i and acceleration a_j, and C(va) is a nonlinear contribution associated with a coupling of velocity and acceleration. Tab. 2 shows that the PBL model privileges the $C(a)$ and $C(va)$ contributions by giving larger values to f_3 and f_4 coefficients than to the coefficients of the other contributions.

2.5.2 Computer Simulation Approach

In general, there are no exact solutions for the traffic cellular automata models we have considered here, except for the cases $v_{max} = 1$ and the low-density behavior of the FI model [19]. Therefore, we used computer simulations to carry out the present study. We developed simple ad hoc code implementations of the NS, FI, and NS+FI traffic cellular automata. One could fix the main model parameters in the programs, such as the size of the lattice, particle density, maximum velocity, randomization probability or stochastic delay, and the maximum number of time steps. We made the computer simulations using an $L = 4000$ sites lattice with periodic boundary conditions. We considered the traffic models with the speed limit $v_{max} = 5$. With each traffic model, we performed 10000 time-step simulations for particle densities n ranging from 0 to 1 with steps $\delta n = 0.05$ and

stochastic delays p ranging from 0 to 1 with steps $\delta p = 0.2$. We carried out computer simulations for several spans T_{max} to verify that the system reached a steady-state condition. We observed that for $T_{max} > 5000$, each model was virtually under a steady-state condition. In this work, we selected $T_{max} = 10000$ to calculate the densities n_i and the acceleration elements A_{ij} ($i = 0, 1, \ldots, 5$ and $j = -5, \ldots -1, 0, 1, \ldots, 5$). We repeated 100 times each simulation, and we calculated the averages of n_i and A_{ij} over the number of simulations for each pair (n, p).

3 Results and Discussion

This section presents the computer simulation results obtained for the steady-state behavior of the NS, FI, and NS+FI traffic cellular automata. Specifically, the velocity and acceleration distributions, the energy consumption, and the CO_2 emission rates.

3.1 Verification of the Steady-State Condition

We carried out computer simulations for several spans to verify that the system reached a steady-state condition:

$$T_{max} = 10, 50, 100, 500, 1000, 5000, 7000, 10000$$

Fig. 1 shows the plots of the partial densities $n_0, n_1, \ldots, n_5$ of the NS velocity distribution for the case $v_{max} = 5$ as functions of the particle density for the stochastic delay $p = 0.6$. These plots suggest the system can be considered virtually under a steady-state condition for $T_{max} > 5000$. We selected $T_{max} = 10000$ for this work.

3.2 Steady-State Velocity and Acceleration Distributions

In this section, we present the velocity and accelerations distributions of the NS, FI and NS+FI traffic cellular automata under virtual steady-state conditions obtained by computer simulations with a speed limit $v_{max} = 5$. These distributions allow to determine the properties of the TCA models, such as the fundamental diagrams (Sec. 3.3), energy consumptions, and CO_2 emissions to the atmosphere, which we presented in the following sections.

3.2.1 NS Model Velocity Distribution

Fig. 2 shows the partial densities $n_0, n_1, \ldots, n_5$ of the NS steady-state velocity distribution for $v_{max} = 5$ as functions of the particle density n and stochastic delay p.

The density n_i gives the number of model vehicles moving with the velocity $v_i = i$, with $i = 0, 1, \ldots, 5$. Here, for any stochastic delay, we observe the number of vehicles at rest n_0 growing from 0 up to 1 as n increases from 0 to 1. The value of p determines the growth rate of n_0 with n, which increases as p increases, with the limit
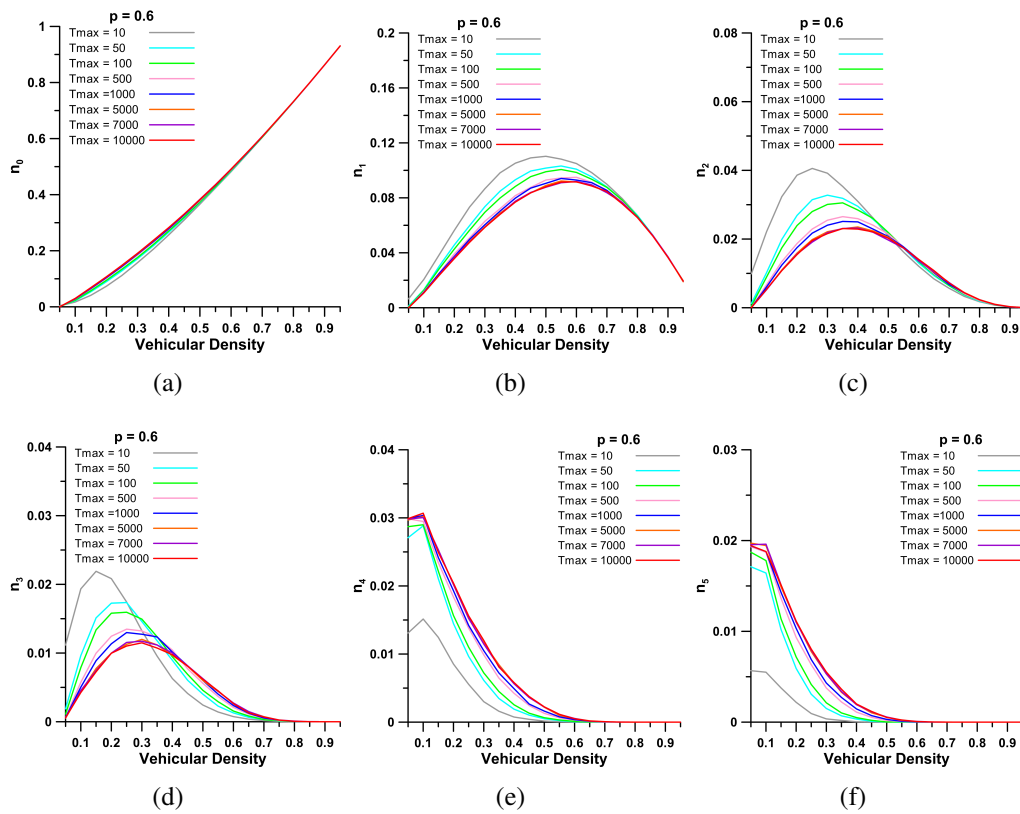
Figure 1 Verification of the steady-state condition. The plots show the partial densities $n_0, n_1, \ldots, n_5$ of the NS model velocity distribution for the case $v_{max} = 5$ as functions of the particle density for $p = 0.6$, and several simulation spans. For $T_{max} > 5000$ the system is virtually under a steady-state condition. (a) n_0, (b) n_1, (c) n_2, (d) n_3, (e) n_4, and (f) n_5.
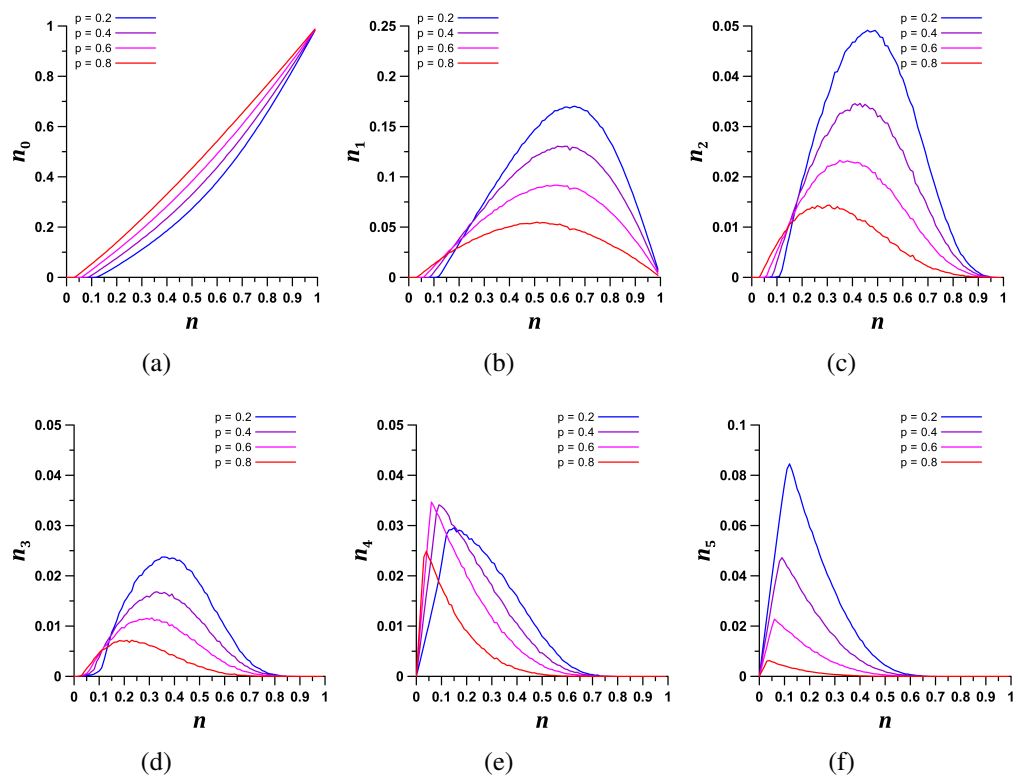
Figure 2 Steady-state velocity distributions of the NS traffic cellular automata as functions of the particle density and stochastic delay. (a) n_0, (b) n_1, (c) n_2, (d) n_3, (e) n_4, and (f) n_5.

$$\lim_{p \to 1} \left(\frac{\partial n_0}{\partial n} \right) = 1 \qquad (23)$$

Equivalently,

$$\lim_{p \to 1} n_0(n, p) = n \qquad (24)$$

The other partial densities $n_1, \ldots, n_5$ have the limits

$$\lim_{n \to 0} n_i(n, p) = \lim_{n \to 1} n_i(n, p) = 0 \qquad (25)$$

for any p. We also observe that n_1, n_2, n_3, and n_5 have peaks with decreasing height as p increases. Otherwise, the partial density n_4 has a peak that grows with p for $p < 0.5$ and shrinks as p increases for $p > 0.5$, approximately.

Under steady-state conditions, the vehicles most abundant are those with the velocities $v_0 = 0$ and $v_1 = 1$, in that order, although with a substantial difference among them. While n_0 grows monotonically from 0 to 1, the partial density n_1 grows from zero to a value less than 0.2 and then decreases to zero again. On the other hand, the vehicles less abundant were those with velocity v_4 with partial density $n_4 < 0.035$.

With the exceptions of n_0 and n_4, all the partial densities decrease as the stochastic delay increases. The partial density n_0 (the fraction of vehicles with $v_0 = 0$) increases with p since this parameter controls the frequency of the vehicles braking. The partial density n_4 has a dependence on the stochastic delay very different than the others. Initially, n_4 grows as p increases, but for values $p > 0.5$, n_4 decreases as p increases. This behavior is due to the fact that the speed limit is $v_{max} = 5$. The particles with velocity $v = 5$ only can remain with this velocity or decelerate to $v = 4$. Moreover, as we will see later (Sec. 3.2.4), for small p the particles with velocity $v = 3$, can accelerate more frequently than decelerate.

3.2.2 FI Model Velocity Distribution

Fig. 3 shows plots of the partial densities $n_0, n_1, \ldots, n_5$ of the steady-state velocity distribution of model FI with $v_{max} = 5$, as functions of the particle density n and stochastic delay p. The density n_i gives the number of model vehicles moving with the velocity $v_i = i$, with $i = 0, 1, \ldots, 5$.

Fig. 3 shows that all the vehicles are moving with one of the two largest velocities, v_4 or v_5, in the low-density modality ($0 < n < \frac{1}{v_{max}}$). In this interval, all the partial densities are equal to zero, excepting v_4 and v_5. A theoretical deduction of this behavior was reported in [19]. Moreover, one detects the effect of the stochastic delay only in the fast particles. For particle densities $n > \frac{1}{v_{max}} = 0.2$, the partial densities revealed no dependence on the stochastics delay. The FI model differs from the NS model in that the increase in speed may not be gradual and that stochastic delay only applies to the fast particles.

3.2.3 NS+FI Model Velocity Distribution

Fig. 4 shows the partial densities $n_0, n_1, \ldots, n_5$ of the NS+FI steady-state velocity distribution for the case $v_{max} = 5$ as functions of the vehicular density and stochastic delay. With
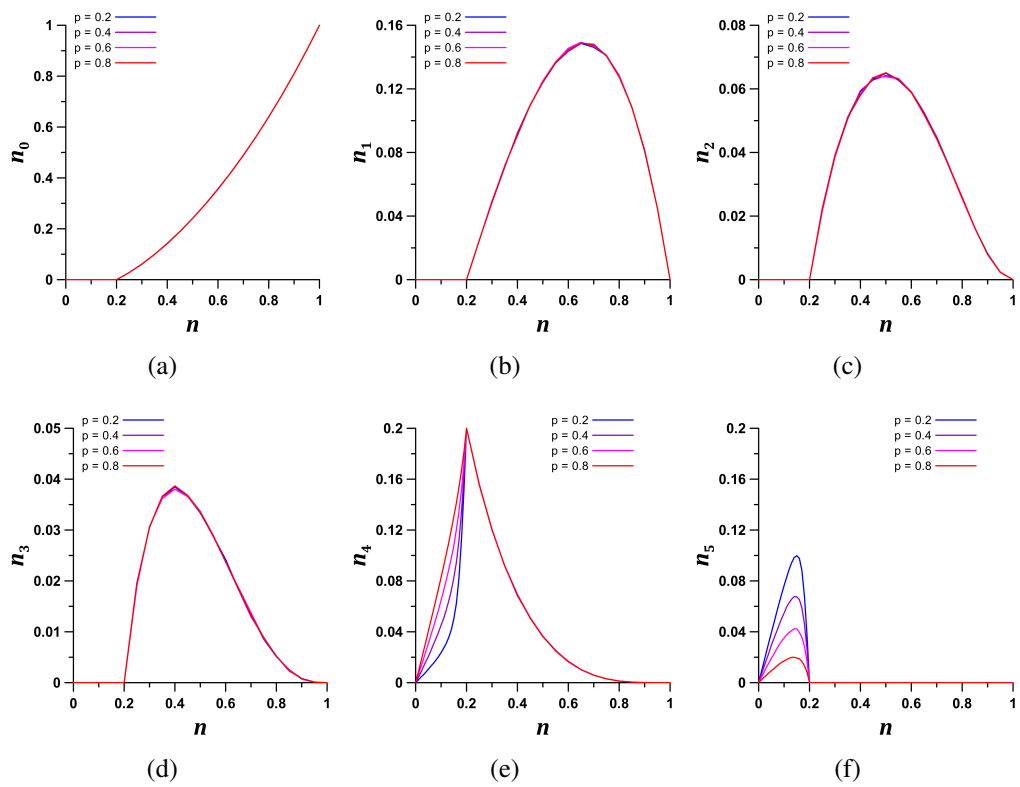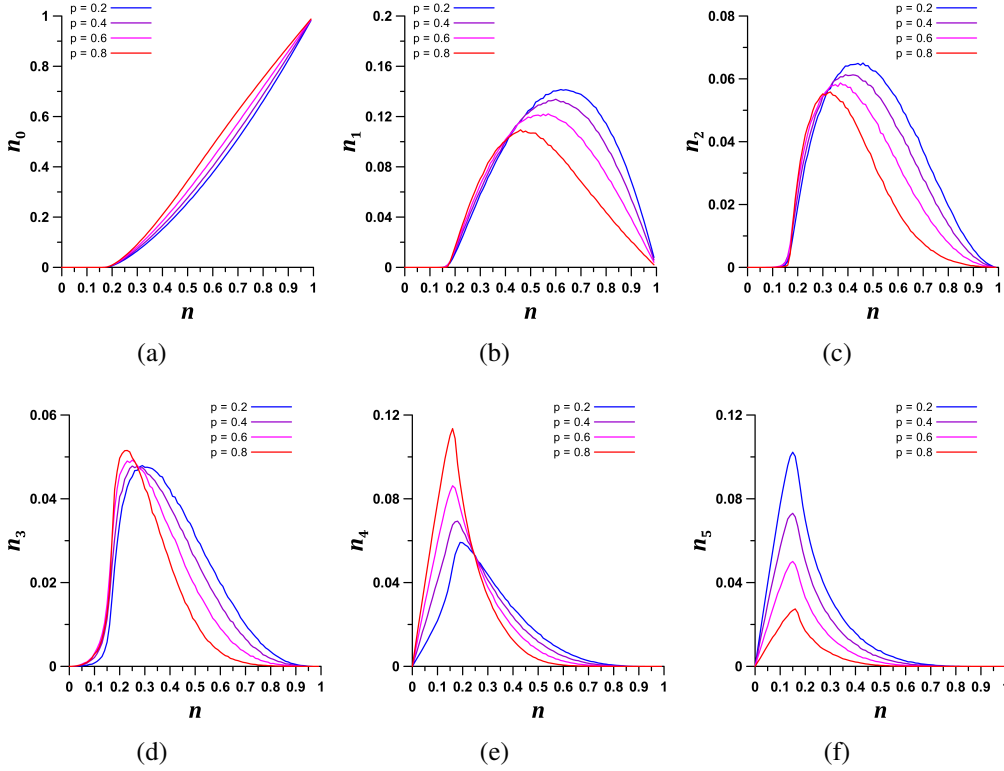
Figure 3 Steady-state velocity distributions of the FI traffic cellular automata as functions of the particle density and stochastic delay. (a) n_0, (b) n_1, (c) n_2, (d) n_3, (e) n_4, and (f) n_5.

Figure 4 Steady-state velocity distributions of the NS+FI traffic cellular automata as functions of the particle density and stochastic delay. (a) n_0, (b) n_1, (c) n_2, (d) n_3, (e) n_4, and (f) n_5.

exception of n_0, all the partial densities in the NS+FI model driving style, under steady-state conditions, are concave functions of n with the same limits as in the NS model given by Eq. 25. In this model, however, the partial densities n_0, n_3, and n_4 increase with p, but n_1, n_2, and n_5 decrease as p increases. The most abundant are the vehicles with the velocities $v_0 = 0$ and $v_1 = 1$. On the other hand, the less abundant were the vehicles with velocities v_2 and v_3, whose partial densities were $n_2 < 0.07$ and $n_3 < 0.06$. Fig. 4 also shows that under low density conditions ($n < 1/v_{max} = 0.2$), almost all vehicles are moving with the larger speeds, v_4 and v_5, as it occurs with the FI driving style.

3.2.4 NS Model Acceleration Distribution

The acceleration distribution matrix **A** has $(v_{max} + 1) \times (2v_{max} + 1)$ elements (66 elements for models with $v_{max} = 5$). The element A_{ij} gives the number of vehicles moving with the velocity $v_i = i$ and acceleration $a_j = j$. In the case of the NS model, the values with $j > 1$ are not possible because of the gradual acceleration style of this TCA (as underlined in Sec. 2.1.1, the velocity of one car can increase only by one each cycle of the updating process). Moreover, all the negative accelerations (braking) are possible from $-i$ to -1 for velocities $v_i > v_0$. Therefore, the only elements $A_{ij} > 0$ are those with $i = 0, 1, \ldots, 5$ and $j = -i, \ldots, 0, 1$. These are 26 elements for the NS model with $v_{max} = 5$.

Fig. 5 shows the elements $A_{ij} > 0$ of the NS steady-state acceleration distribution for the case $v_{max} = 5$ for several values of the vehicular density n and stochastic delays $p = 0.2, 0.6, 0.8$. In the Fig. 5, Fig. 6, and Fig. 7, we denoted the fractions A_{ij} as $A[i,j]$.

In Fig. 5, we observe the reason why n_4 grows as p increases while $p < 0.5$, but decreases for values $p > 0.5$. The acceleration elements A_{50} and A_{5-1} of the vehicles with velocity $v = 5$ indicate that these vehicles only can remain with this velocity or decelerate to $v = 4$ (decelerations to smaller velocities are practically negligible). Moreover, the elements A_{3j} of the vehicles with velocity $v = 3$ show that these vehicles accelerate more frequently than decelerate.

3.2.5 FI Model Acceleration Distribution

As in the NS model, the FI model transition rules limited the number of elements of the acceleration distribution matrix that can be larger than zero in the case $v_{max} = 5$. In this case we obtained 28 elements $A_{ij} > 0$. Fig. 6 shows these elements as functions of the particle density n for $p = 0.2, 0.6, 0.8$. In Fig. 6, we observed that for particle densities $n > \frac{1}{v_{max}} = 0.2$, all the fractions A_{ij} do not depend on the stochastic delay. For low-densities ($0 < n < 0.2$), however, the only elements $A_{ij} > 0$ are A_{40}, A_{41}, A_{50}, and A_{5-1}, with values dependent on the stochastic delay.

3.2.6 NS+FI Model Acceleration Distribution

In this case we obtained 30 elements $A_{ij} > 0$, which correspond to $j = -i, \ldots, 0, \ldots, 5-i$. Fig. 7 shows the plots of these elements as functions of density n for $p = 0.2, 0.6, 0.8$. In Fig. 7, we observed that all the fractions A_{ij} present a clear dependence on the stochastic delay. For low-densities ($0 < n < 0.2$), the elements A_{0j}, A_{1j}, and A_{2j} are negligibly small or small for any p. Otherwise, A_{40}, A_{41}, A_{50}, and A_{5-1} have considerable values within the same density interval.

3.3 Steady-State Fundamental Diagrams

From Eq. 4, we determined the mean vehicular flow per site q for the NS, FI, and NS+FI models. Fig. 8(a,b,c) present the fundamental diagrams (q as a function of vehicular density n) and Fig. 8(d,e,f) show the mean velocities, $\bar{v} = q/n$, under (virtually) steady-state conditions for several stochastic delay values.

For the NS model, the vehicular flows q_{NS}, q_{FI}, and q_{NSFI}, are increasing then decreasing functions of the vehicular density, with their maximum values located in the low-density region, $n \leq \frac{1}{v_{max}}$. The peak of the vehicular flow q_{NS} decreases with the stochastic delay. For $p = 0$, the peak value is $q_{NS} = 0.8$, at $n = \frac{1}{v_{max}} = 0.2$. In the case of the FI and NS+FI driving styles, the vehicular flows q_{FI} and q_{NSFI} are very slight decreasing functions of the stochastic delay for low densities $n < \frac{1}{v_{max}} = 0.2$. For high densities ($n > 0.2$), the flow q_{FI} only depends on n, and is given by $q_{FI} = 1 - n$. In the case of the NS+FI model, q_{NSFI} is a decreasing function with both, n and p. The driving style with
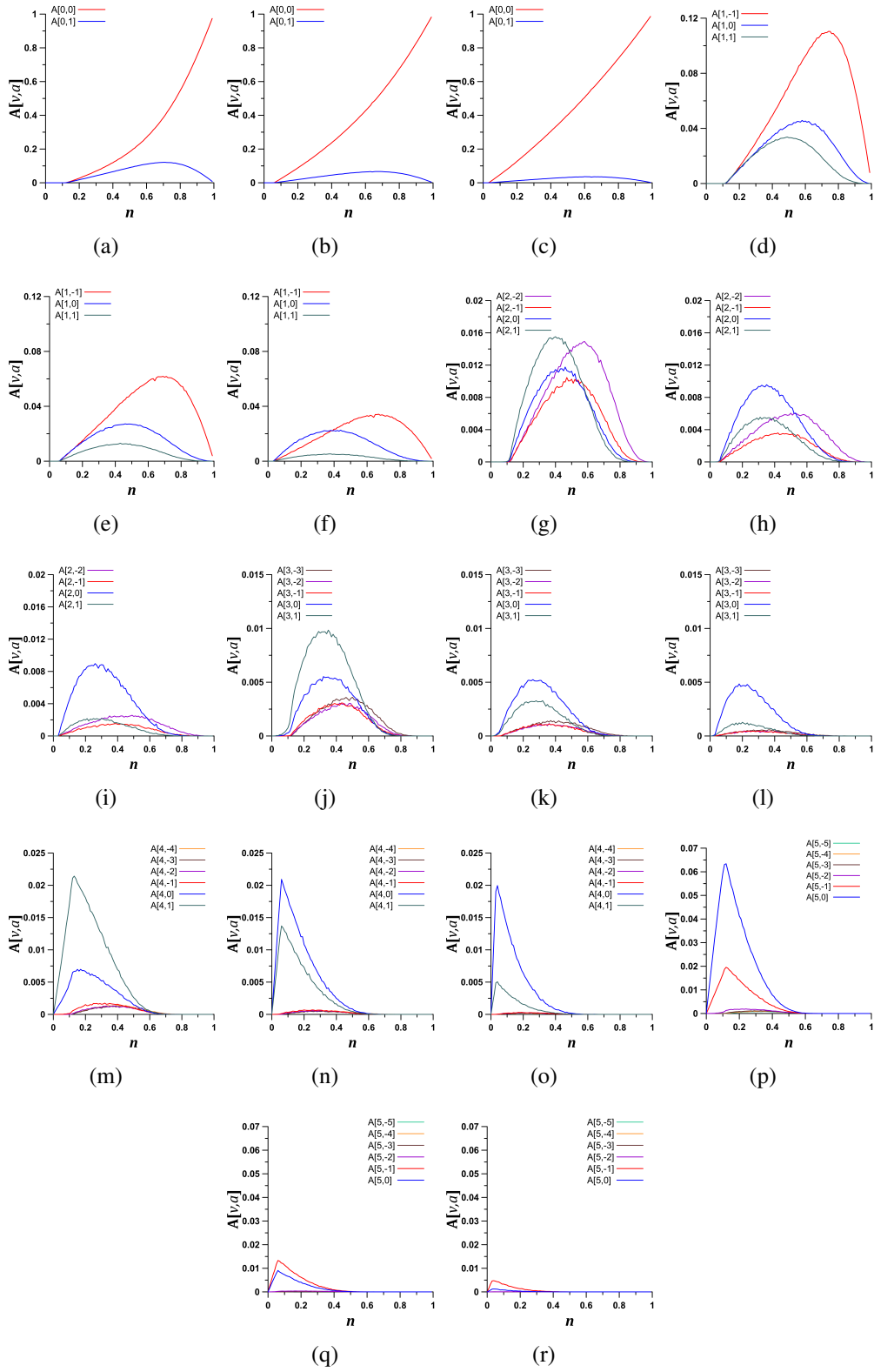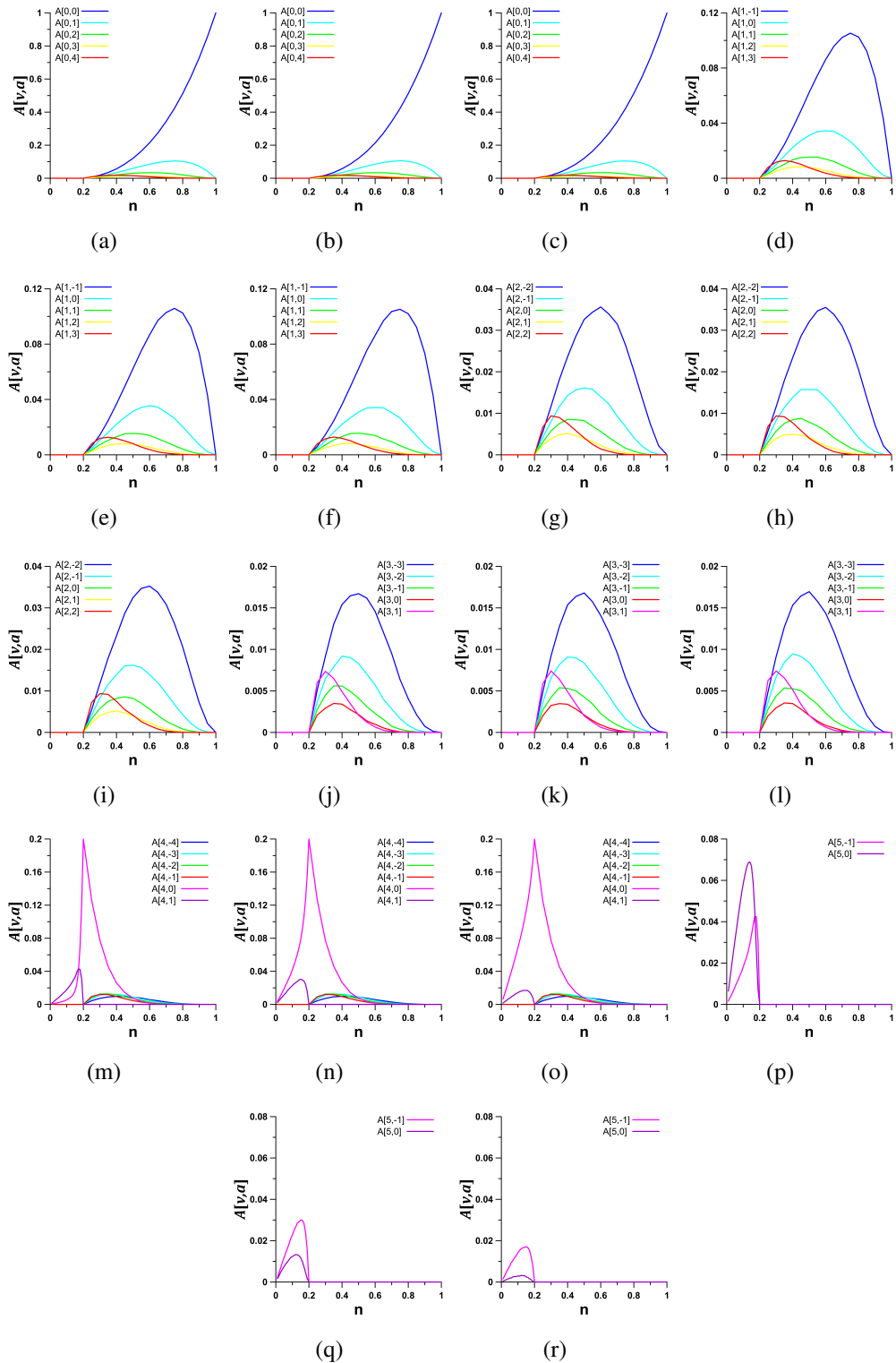
Figure 5 Steady-state acceleration distribution for the NS model with $v_{max} = 5$. (a) A_{0j}, $p = 0.2$; (b) A_{0j}, $p = 0.6$; (c) A_{0j}, $p = 0.8$; (d) A_{1j}, $p = 0.2$; (e) A_{1j}, $p = 0.6$; (f) A_{1j}, $p = 0.8$; (g) A_{2j}, $p = 0.2$; (h) A_{2j}, $p = 0.6$; (i) A_{2j}, $p = 0.8$; (j) A_{3j}, $p = 0.2$; (k) A_{3j}, $p = 0.6$; (l) A_{3j}, $p = 0.8$; (m) A_{4j}, $p = 0.2$; (n) A_{4j}, $p = 0.6$; (o) A_{4j}, $p = 0.8$; (p) A_{5j}, $p = 0.2$; (q) A_{5j}, $p = 0.6$; (r) A_{5j}, $p = 0.8$.
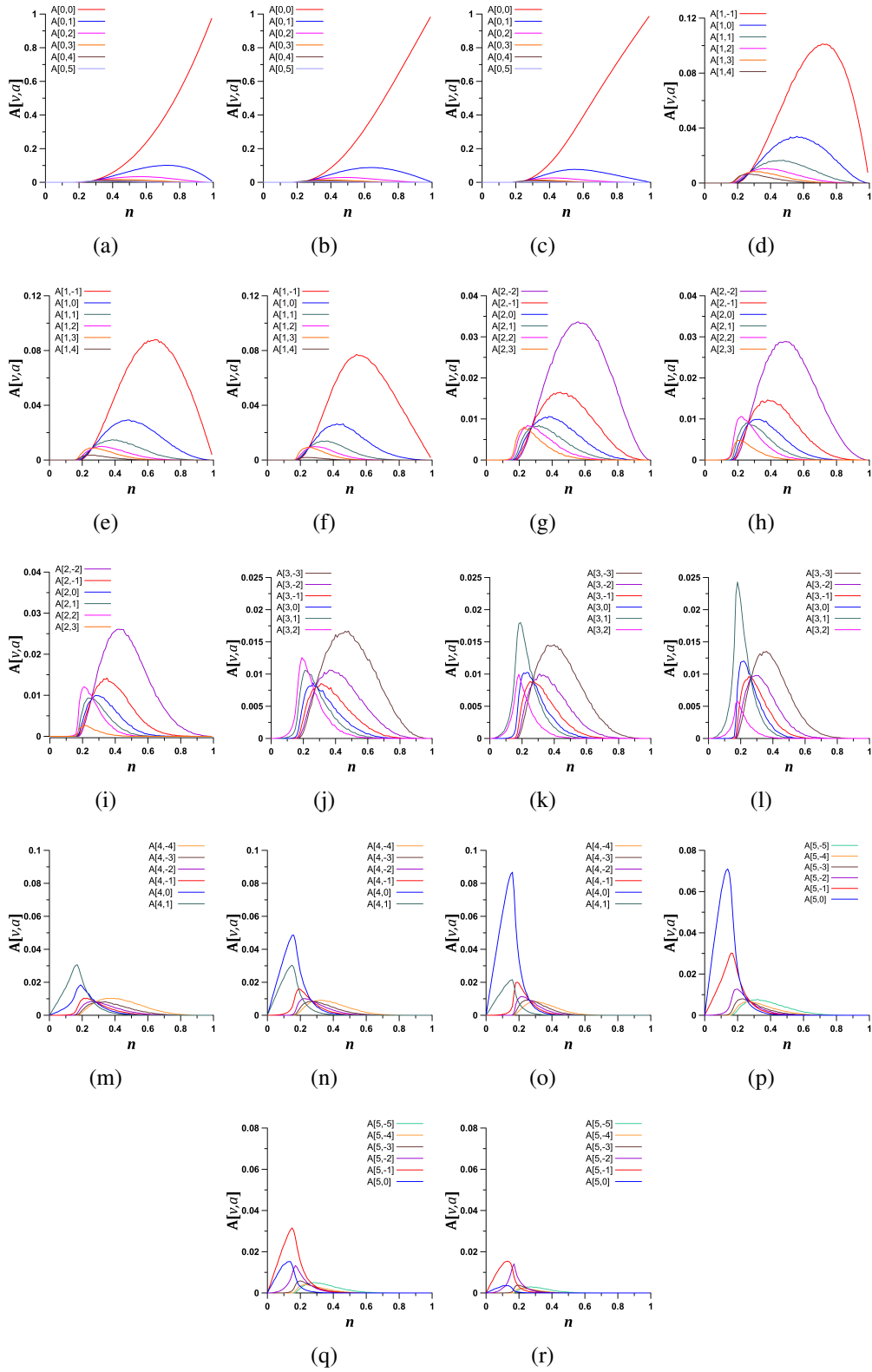
Figure 6 Steady-state acceleration distribution for the FI model with $v_{max} = 5$. (a) A_{0j}, $p = 0.2$; (b) A_{0j}, $p = 0.6$; (c) A_{0j}, $p = 0.8$; (d) A_{1j}, $p = 0.2$; (e) A_{1j}, $p = 0.6$; (f) A_{1j}, $p = 0.8$; (g) A_{2j}, $p = 0.2$; (h) A_{2j}, $p = 0.6$; (i) A_{2j}, $p = 0.8$; (j) A_{3j}, $p = 0.2$; (k) A_{3j}, $p = 0.6$; (l) A_{3j}, $p = 0.8$; (m) A_{4j}, $p = 0.2$; (n) A_{4j}, $p = 0.6$; (o) A_{4j}, $p = 0.8$; (p) A_{5j}, $p = 0.2$; (q) A_{5j}, $p = 0.6$; (r) A_{5j}, $p = 0.8$.
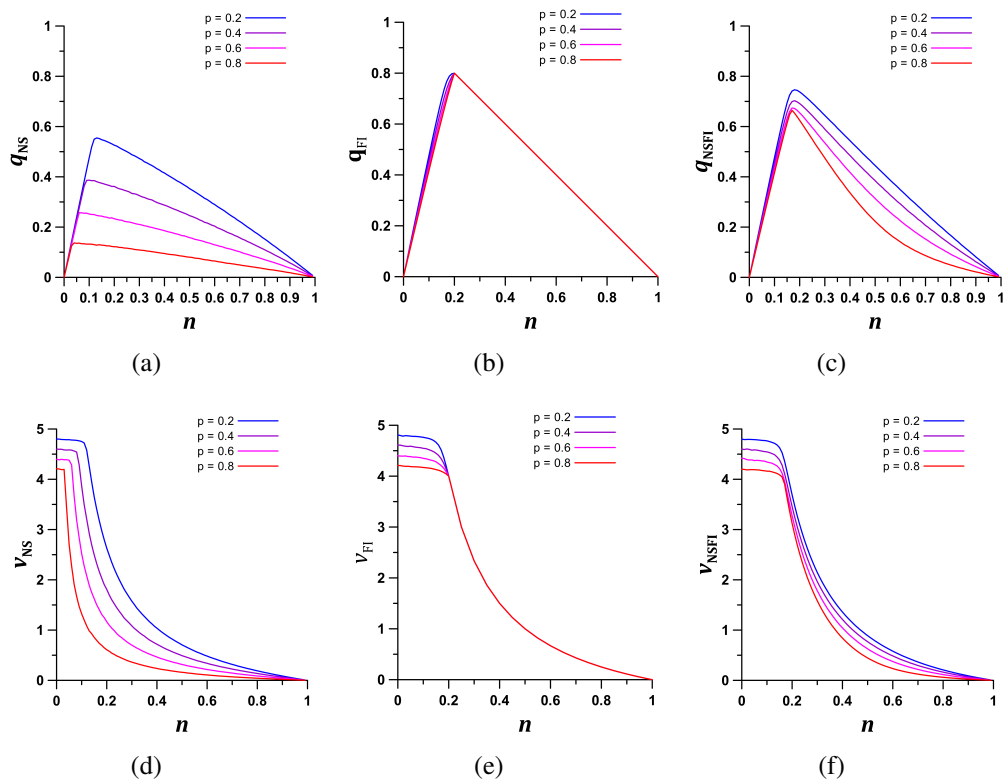
Figure 7 Steady-state acceleration distribution for the NS+FI model with $v_{max} = 5$. (a) A_{0j}, $p = 0.2$; (b) A_{0j}, $p = 0.6$; (c) A_{0j}, $p = 0.8$; (d) A_{1j}, $p = 0.2$; (e) A_{1j}, $p = 0.6$; (f) A_{1j}, $p = 0.8$; (g) A_{2j}, $p = 0.2$; (h) A_{2j}, $p = 0.6$; (i) A_{2j}, $p = 0.8$; (j) A_{3j}, $p = 0.2$; (k) A_{3j}, $p = 0.6$; (l) A_{3j}, $p = 0.8$; (m) A_{4j}, $p = 0.2$; (n) A_{4j}, $p = 0.6$; (o) A_{4j}, $p = 0.8$; (p) A_{5j}, $p = 0.2$; (q) A_{5j}, $p = 0.6$; (r) A_{5j}, $p = 0.8$.

Figure 8 Fundamental diagrams for the traffic cellular automata under (virtually) steady-state conditions. (a) and (d) NS model, (b) and (e) FI model, (c) and (f) NS+FI model.
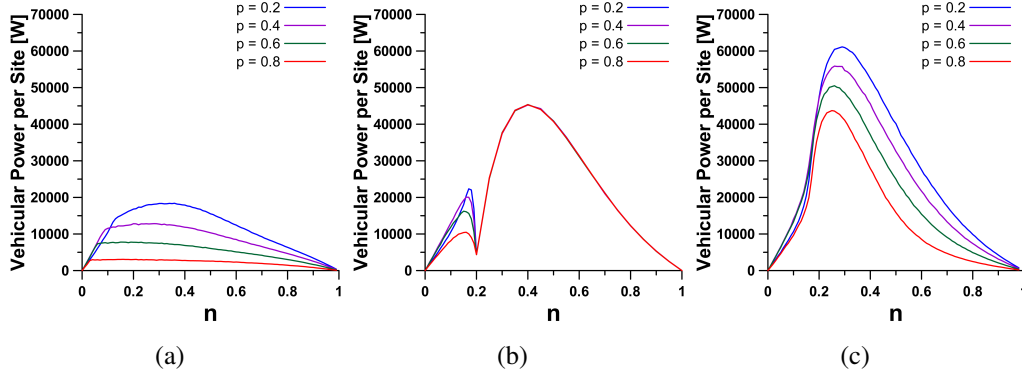
Figure 9   Steady-state vehicular power per site in traffic cellular automata. (a) NS model, (b) FI model, (c) NS+FI model.

the larger vehicular flow was that of the FI model, followed by the flows of the NS+FI and NS models.

From the vehicular flows $q_{NS}(n,p)$, $q_{FI}(n,p)$, and $q_{NSFI}(n,p)$, we calculated the mean velocities $\bar{v}$ using Eq. 4. Fig. 8(d,e,f) show the plots of the mean velocities $\bar{v}_{NS}(n,p)$, $\bar{v}_{FI}(n,p)$, and $\bar{v}_{NSFI}(n,p)$, for $p = 0.2, 0.4, 0.6, 0.8$. Here, we observe, for the FI and NS+FI models, that the mean velocities remain almost constant for $n < 0.2$, and decrease as n increases for $n > 0.2$. For $p = 0.2$, the average values of $\bar{v}_{NS}$, $\bar{v}_{FI}$, and $\bar{v}_{NSFI}$ were 1.43, 1.87, and 1.68 sites per time step, which, according to Eq. 16, correspond to 38.61, 50.49, and $45.36 km/h$ for the NS, FI and NS+FI models.

3.4 Steady-State Energy Consumption Rate in TCA

For the TCA models with $v_{max} = 5$ that we have considered, Fig. 9 presents the steady-state vehicular power (or energy consumption per unit time) per site, $P(n,p)$, for several values of n and $p = 0.2, 0.4, 0.6, 0.8$. We calculated $P(n,p)$ using Eq. 15, the steady-state velocity and acceleration distributions, $n_i(n,p)$ and $A_{ij}(n,p)$ previously described in Sec. 3.2, and the vehicle characteristics given in Tab. 1. The plots of Fig. 9 do not include a contribution due to the basic energy consumption by a vehicle stopped with the engine running or electric consumers such as lights or air conditioning.

In Fig. 9(a) and Fig. 9(c), we observe that the vehicular power per site in the NS and NS+FI models reflects a strong dependence on the stochastic delay, where $P_{NS}(n,p)$ and $P_{NSFI}(n,p)$ decrease as p increases. This behavior is partially a consequence of the fact that the larger values of n_i correspond, in general, to the smaller values of p, except for the vehicles at rest (Fig. 2).

In Fig. 9(b), otherwise, we observe that the vehicular power per site in the FI model, $P_{FI}(n,p)$, only depends on the stochastical delay for densities $n < \frac{1}{v_{max}}$. In the low-density behavior ($n < 0.2$), this model has all the vehicles moving with the highest velocities v_4 and v_5, and therefore the vehicles with smaller velocities, v_0, v_1, v_2 and v_3, do not contribute to the vehicular power per site of the system (see Sec. 3.2.2, Fig. 3). When
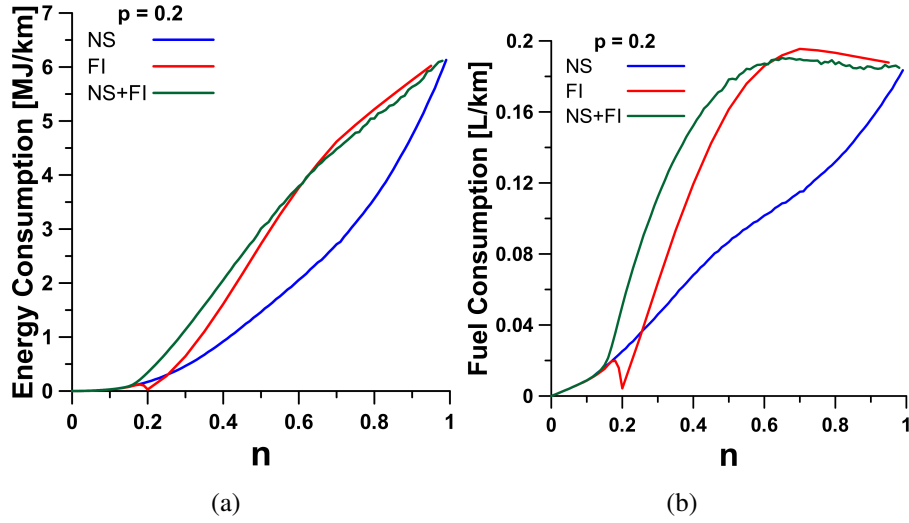
Figure 10   Energy (a) and fuel (b) consumption per kilometer with the NS, FI, and NS+FI driving styles for the stochastic delay $p = 0.2$.

density is $n = \frac{1}{v_{max}} = 0.2$, the cars are distributed uniformly in the lattice (one car every fifth cell), each one moving with velocity $v = 4$. In this case, a synchronized traffic flow condition prevails with no acceleration, and the energy consumption sustains the motion against aerodynamic and rolling dissipation. For $n > 0.2$, all the cars are at rest or moving with the velocities v_1, v_2, v_3, and v_4 (there are no vehicles with velocity v_5), being the cars with velocities v_1 and v_4 those with the more substantial contributions to vehicular power.

The plots in Fig. 9 reveal that the energy consumption rate per site in the NS model is considerably smaller than in the FI and NS+FI models. For $p = 0.2$, $P_{NS}(n, p)$ reaches its maximum of $18.35kW$ for n close to 0.35. In the FI model we found that $P_{FI}(n, p)$ reaches its maximum of $45.35kW$ for n close to 0.4, independently of p, and in the NS+FI model, for $p = 0.2$, $P_{NSFI}(n, p)$ reaches its maximum of $61.10kW$ for $n = 0.3$. On average, for $p = 0.2$, the energy consumption rates per site were 11.2, 21.8, and $26.9kW$ for the NS, FI, and NS+FI models, respectively.

In Fig. 10, we presented the energy and fuel (petrol) consumption per kilometer for the NS, FI, and NS+FI models, for $p = 0.2$. From Fig. 10(a,b), for the energy consumption we obtained the average values of 1.88, 2.60, and $2.76MJ/km$, and for the fuel consumption we obtained the average values of 0.08, 0.12, and $0.13L/km$, for the NS, FI, and NS+FI models It is interesting to underline that for petrol, typical values of density and caloric value are $750kg/m^3$ and $45MJ/Kg$, which, for a highway fuel consumption of $10km/L$, give an energy consumption of $3.37MJ/km$.

3.5 Steady-State CO_2 Emission Rate in TCA

Fig. 11 shows the steady-state CO_2 emission rate per lattice site, $G(n, p)$, for the NS, FI, and NS+FI traffic models with $v_{max} = 5$. The CO_2 emission rates were calculated using Eq. 18, the steady-state velocity and acceleration distributions $n_i(n, p)$ and $A_{ij}(n, p)$
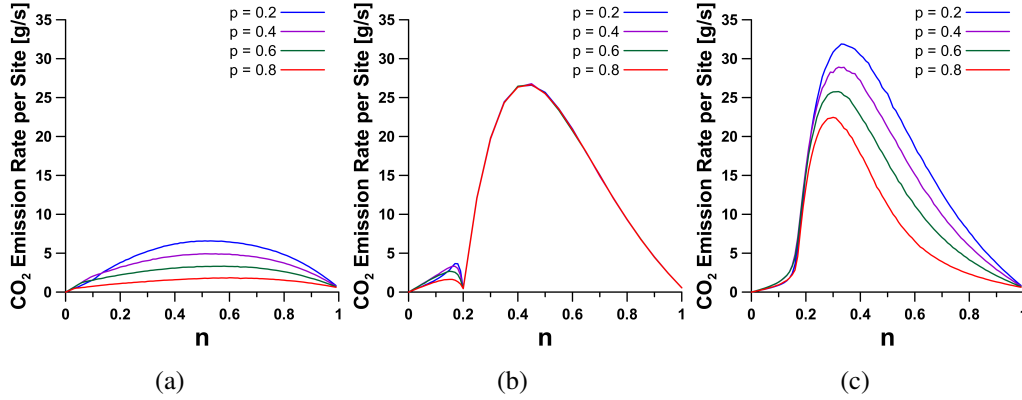
Figure 11   Steady-state CO$_2$ emission rate per site in traffic cellular automata. (a) NS model, (b) FI model, (c) NS+FI model.
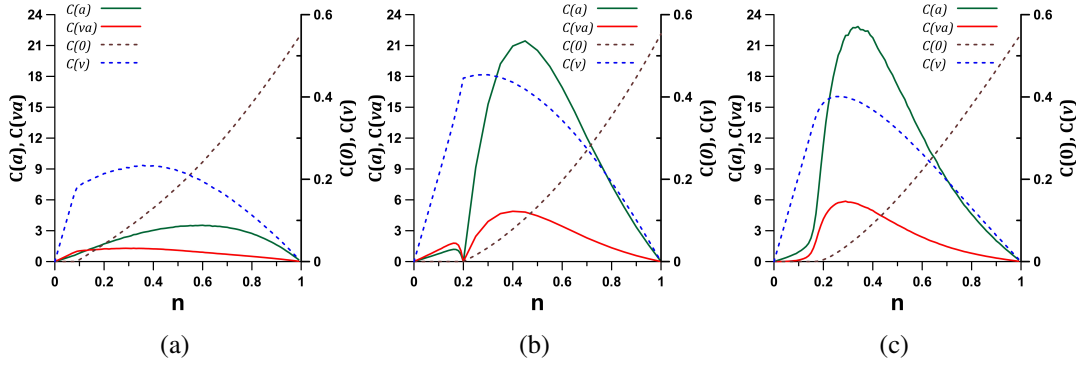

Figure 12   Contributions of the vehicles velocity and acceleration to the steady-state CO$_2$ emission rate per site (g/s) in traffic cellular automata. (a) NS model, (b) FI model, (c) NS+FI model.

described in Sec. 3.2, and the emission constants for a gasoline engine given in Tab. 2. With the NS and NS+FI driving style models, the CO$_2$ emission rates per site reflect the effect of the stochastic delay, decreasing as p increases. In the case of the FI model, we only detected an effect of the stochastic delay for low vehicular densities $n < 0.2$, but no dependence was observed for larger densities.

The individual contributions of vehicles velocity and acceleration to the CO$_2$ emission rate per site are shown in Fig. 12 (expressed in g/s) for the NS, FI, and NS+FI traffic models. In this figure, we observe that the acceleration contributions to the emission rate per site are close to two orders of magnitude larger than the velocity contributions.

In magnitud, we observed that the larger emissions were produced by the NS+FI driving style model, and the smaller by the NS model. For $p = 0.2$, we obtained the following peak values of the emissions rates per site, $G_{NS} = 6.6 g/s$ for $n = 0.5$, $G_{FI} = 26.6 g/s$ for $n = 0.45$, and $G_{NSFI} = 31.9 g/s$ for $n = 0.33$. On average, for $p = 0.2$, the CO$_2$ emission rates per site were 4.42, 12.66, and 14.51 g/s for the NS, FI and NS+FI models.

In Fig. 13, we presented the plots of the CO$_2$ emission per kilometer as a function of density, for the NS, FI and NS+FI models with $p = 0.2$. Here, the average values were
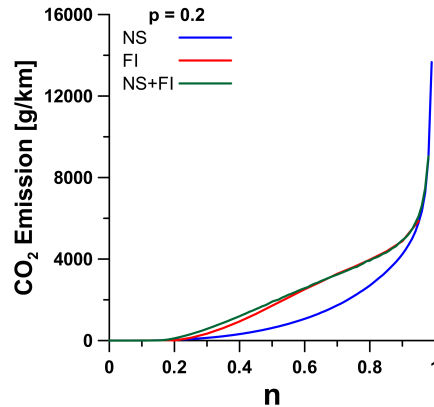
Figure 13 CO_2 emission per kilometer with the NS, FI, and NS+FI driving styles for the stochastic delay $p = 0.2$.

1.37, 1.93, and 2.14$kgCO_2/km$. Now, we have to observe that, according to the EPA emission factor of 2.35$kgCO_2/l$ [42], the CO_2 emission of a car with a fuel consumption of 10km/l is 0.235$kgCO_2/km$. It must be observed, however, that the averaging here has considered the full density interval $0 < n < 1$. For $v_{max} = 5$, densities $n > 1/v_{max} = 0.2$ do not correspond already to free flow conditions. Then, as it is observed in Fig. 13, in the limit $n \rightarrow 1$, the strong jamming condition produces very large CO_2 emission per kilometer since $\bar{v} \rightarrow 0$. In fact, if we only take in to account densities $n < 0.5$, the average values of CO_2 emission are 0.158, 0.460, and 0.562$kgCO_2/km$.

4 Conclusions

This paper studied the energy consumption and CO_2 emissions of vehicular traffic from the TCA standpoint. The transition rules of the traffic models proposed by Nagel and Schreckenberg [4], Fukui and Ishibashi [5], and Fu et al. [49] were considered as representatives of different driving styles, then computer simulations were carried out with these TCA to evaluate their effect on their energy and fuel consumption and CO_2 emissions under steady-state conditions for different values of stochastic delay. Driving style generally refers to the way a driver prefers to or habitually drives the car. The driving style can be classified into three typical types [56]: aggressive type, moderate type, and cautious type. The aggressive driving style is usually associated with high speed and hard acceleration, as it occurrs in the FI model. In contrast, a cautious driver would drive more carefully, avoiding high speed, and accelerating gradually. Cautious driving style is usually associated with longer space headway and longer deceleration. We considered the NS model as a representative of a cautious style. The moderate driver drives with relative steady motions that are neither too cautious nor too aggressive, as it is the case in the NS+FI model. The energy consumption was estimated with an extension of the Newton formula for the power developed by the tractive force required to accelerate the vehicle against the aerodynamic and rolling resistance. The CO_2 emissions were esti-

mated extending the Int Panis et al. empirical model [37] to TCA. Both methods require the steady-state distributions of velocity and acceleration, and we obtained them from computer simulations. From a methodological standpoint, these extended methods constitute original contributions for estimating energy consumption and pollutant emissions of vehicular traffic using TCA simulations. Some quantitative results: For the NS, FI, and NS+FI models with an stochastic delay $p = 0.2$, we obtained average values of 1.88, 2.60, and $2.76 MJ/km$ of energy consumption, average values of 0.08, 0.12, and $0.13 L/km$ of fuel consumption, and average values (over the density interval of $0 < n < 0.5$) of 0.158, 0.460, and $0.562 kgCO_2/km$ for the CO$_2$ emissions. For petrol combustion engines, it is interesting to underline that typical values of density and caloric value are $750 kg/m^3$ and $45 MJ/Kg$, which, for a highway fuel consumption of $10 km/L$, give an energy consumption of $3.37 MJ/km$. Also, we underline that, according to the EPA emission factor of $2.35 kgCO_2/l$ [42], the CO$_2$ emission of a car with a fuel consumption of $10 km/l$ is $0.235 kgCO_2/km$. This work shows that the traffic cellular automata can help evaluate energy consumption scenarios and vehicular emissions under different traffic flow and driving style conditions in order to optimize the traffic flow and mitigate its adverse impacts on air quality and climate.

A final comment. Traffic cellular automata, so as the cellular automaton fluids, belong to the class of dynamical systems known as lattice gases. These are fundamentally discrete systems which can be easely implemented in a computer and simulated precisely. Lattice gases, unlike the computational fluid dynamics models, are not based on approximating partial differential equations to solve them nummerically using some form of discrete mesh in space and time, arguing that when the mesh becomes small enough, correct results would be obtained. Even their conceptual simplicity, lattice gases have often proved extremely useful in practice, but for being models, they are inevitably incomplete, and it is never in any definitive sense possible to establish their validity. Our modeling approach for studying emissions and energy consumption in vehicular traffic provided results that may not give a precise distinction between different realistic driving styles, but definitively it showed that, within the framework of the basic TCA models, emissions and energy consumption are influenced by the driving style, and therefore, this modeling approach may help in defining strategies to assess possible optimizing scenarios.

References

[1] R.A. Alpher: Robert Herman. Physics Today **50**, 77 (1997). doi:10.1063/1.881863.

[2] I. Prigogine, R.C. Herman: Kinetic Theory of Vehicular Traffic. Elsevier (1971).

[3] M. Cremer, J. Ludwig: A fast simulation model for traffic flow on the basis of boolean operations. Mathematics and Computers in Simulation **28**, 297-303. doi:10.1016/0378-4754(86)90051-0.

[4] K. Nagel, M. Schreckenberg: A cellular automaton model for freeway traffic. J. Phys. I. **2** 2221–2229 (1992). doi:10.1051/jp1:1992277.

[5] M. Fukui, Y. Ishibashi: Traffic Flow in 1D Cellular Automaton Model Including Cars Moving with High Speed. J. Phys. Soc. Japan. **65** 1868–1870 (1996). doi:10.1143/JPSJ.65.1868.

[6] D. Chowdhury, L. Santen, A. Schadschneider: Statistical physics of vehicular traffic and some related systems. Phys. Rep. **329** 199–329 (2000). doi:10.1016/S0370-1573(99)00117-9.

[7] D. Helbing: Traffic and related self-driven many-particle systems. Rev. Mod. Phys. **73** 1067–1141 (2001). doi:10.1103/RevModPhys.73.1067.

[8] T. Nagatani: The physics of traffic jams. Reports Prog. Phys. **65** 1331–1386 (2002). doi:10.1088/0034-4885/65/9/203.

[9] K. Nagel, P. Wagner, R. Woesler: Still Flowing: Approaches to Traffic Flow and Traffic Jam Modeling. Oper. Res. **51** 681–710 (2003). doi:10.1287/opre.51.5.681.16755.

[10] R. Barlovic, L. Santen, A. Schadschneider, M. Schreckenberg: Metastable states in cellular automata for traffic flow. Eur. Phys. J. B. **5** 793–800 (1998). doi:10.1007/s100510050504.

[11] O. Biham, A.A. Middleton, D. Levine: Self-organization and a dynamical transition in traffic-flow models. Phys. Rev. A. **46** R6124–R6127 (1992). doi:10.1103/PhysRevA.46.R6124.

[12] B.-H. Wang, L. Wang, P.M. Hui: One-Dimensional Fukui-Ishibashi Traffic Flow Model. J. Phys. Soc. Japan. **66** 3683–3684 (1997). doi:10.1143/JPSJ.66.3683.

[13] R. Jiang, M.-B. Hu, H.M. Zhang, Z.-Y. Gao, B. Jia, Q.-S. Wu, B. Wang, M. Yang: Traffic Experiment Reveals the Nature of Car-Following. PLoS One. **9** e94351 (2014). doi:10.1371/journal.pone.0094351.

[14] K. Ahn, H. Rakha, A. Trani, M. Van Aerde: Estimating Vehicle Fuel Consumption and Emissions based on Instantaneous Speed and Acceleration Levels. J. Transp. Eng. **128** 182–190 (2002). doi:10.1061/(ASCE)0733-947X(2002)128:2(182).

[15] A. Danczyk, D. Levinson, V. der Hoorn: Fundamentals of Transportation/Grade. WIKIBOOKS (2009). http://en.wikibooks.org/w/index.php?oldid=1436014.

[16] H. Rakha, I. Lucic, S.H. Demarchi, J.R. Setti, M. Van Aerde: Vehicle Dynamics Model for Predicting Maximum Truck Acceleration Levels. J. Transp. Eng. **127** 418–425 (2001). doi:10.1061/(ASCE)0733-947X(2001)127:5(418).

[17] K. Zhang, H.C. Frey: Road Grade Estimation for On-Road Vehicle Emissions Modeling Using Light Detection and Ranging Data. J. Air Waste Manage. Assoc. **56** 777–788 (2006). doi:10.1080/10473289.2006.10464500.

[18] K. Nagel: Particle hopping models and traffic flow theory. Phys. Rev. E. **53** 4655–4672 (1996). doi:10.1103/PhysRevE.53.4655.

[19] A. Salcido, E. Hernández-Zapata, S. Carreón-Sierra: Exact results of 1D traffic cellular automata: The low-density behavior of the Fukui–Ishibashi model. Phys. A Stat. Mech. Its Appl. **494** 276–287 (2018). doi:10.1016/j.physa.2017.11.162.

[20] A. Schadschneider, M. Schreckenberg: Cellular automation models and traffic flow. J. Phys. A. Math. Gen. **26** L679–L683 (1993). doi:10.1088/0305-4470/26/15/011.

[21] M. Schreckenberg, A. Schadschneider, K. Nagel, N. Ito: Discrete stochastic models for traffic flow. Phys. Rev. E. **51** 2939–2949 (1995). doi:10.1103/PhysRevE.51.2939.

[22] L.C.Q. Vilar, A.M.C. de Souza: Cellular automata models for general traffic conditions on a line. Phys. A Stat. Mech. Its Appl. **211** 84–92 (1994). doi:10.1016/0378-4371(94)90069-8.

[23] B.A. Toledo, E. Cerda, J. Rogan, V. Munoz, C. Tenreiro, R. Zarama, J.A. Valdivia: Phys. Rev. E 75 026108 (2007). doi:10.1103/PhysRevE.75.026108.

[24] W. Shi, Y. Xue: Study on stability and energy consumption in typical car-following models. Physica A **381** (2007) 399–406. doi:10.1016/j.physa.2007.02.106.

[25] W. Zhang, W. Zhang, X. Yang: Energy dissipation in the deterministic and nondeterministic Nagel–Schreckenberg models. Phys. A Stat. Mech. Its Appl. **387** 4657–4664 (2008). doi:10.1016/j.physa.2008.04.004.

[26] W.-X. Zhu. Analysis of CO$_2$ emission in traffic flow and numerical tests. Physica A **392** 4787–4792 (2013). doi:10.1016/j.physa.2013.06.024.

[27] T.Q. Tang, J.G. Li, Y.P. Wang, G.Z. Yu: Vehicle's fuel consumption of car-following models. Science China Technological Sciences **56** 1307-1312 (2013). doi:10.1007/s11431-013-5182-9.

[28] T.Q.Tang, J.G.Li, H.J.Huang, X.B.Yang: A car-following model with real-time road conditions and numerical tests. Measurement **48** 63-76 (2014). doi:10.1016/j.measurement.2013.10.035.

[29] Y. Xue, S.-J. Kang, W.-Z. Lu, H.-D. He: Energy dissipation of traffic flow at an on-ramp. Physica A **398** (2014) 172–178. doi:10.1016/j.physa.2013.12.032.

[30] T.Q. Tang, J.G. Li, S.C. Yang, H.Y. Shang: Effects of on-ramp on the fuel consumption of the vehicles on the main road under car-following model. Physica A **419** 293–300 (2015). doi:10.1016/j.physa.2014.10.051.

[31] T.Q. Tang, Z.Y. Yi, Q.F. Lin: Effects of signal light on the fuel consumption and emissions under car-following model. Physica A **469** 200–205 (2017) doi:10.1016/j.physa.2016.11.025.

[32] Z. Jin, Z. Yang, H. Ge: Energy consumption investigation for a new car-following model considering driver's memory and average speed of the vehicles. Physica A **506** 1038–1049 (2018). doi:10.1016/j.physa.2018.05.034.

[33] X. Ma, H. Ge, R. Cheng: Influences of acceleration with memory on stability of traffic flow and vehicle's fuel consumption. Physica A **525** 143–154 (2019). doi:10.1016/j.physa.2019.03.024.

[34] Y. Xue, X. Wang, B. Cen, P. Zhang, H. He: Study on fuel consumption in the Kerner–Klenov–Wolf three-phase cellular automaton traffic flow model. Nonlinear Dyn. **102** 393–402 (2020). doi:10.1007/s11071-020-05947-2.

[35] Y. Qiao, Y. Xue, X. Wang, B. Cen, Y. Wang, W. Pan, Y. Zhang: Investigation of PM emissions in cellular automata model with slow-to-start effect. Phys. A Stat. Mech. Its Appl. **574** 125996 (2021). doi:10.1016/j.physa.2021.125996.

[36] M. Takayasu, H. Takayasu: 1/f Noise in a Traffic Model. Fractals **01** 860–866 (1993). doi:10.1142/S0218348X93000885.

[37] L. Int Panis, S. Broekx, R. Liu: Modelling instantaneous traffic emission and the influence of traffic speed limits. Sci. Total Environ. **371** 270–285 (2006). doi:10.1016/j.scitotenv.2006.08.017.

[38] N. Lakouari, O. Oubram, A. Bassam, S.E. Pomares Hernandez, R. Marzoug, H. Ez-Zahraouy: Modeling and simulation of CO_2 emissions in roundabout intersection. J. Comput. Sci. **40** 101072 (2020).doi:10.1016/j.jocs.2019.101072.

[39] H. Binoua, H. Ez-Zahraouy, A. Khallouk, N. Lakouari: Carbon dioxide emission in a single-lane cellular automaton model with a series of traffic lights. Int. J. Mod. Phys. C. **31** 2050154 (2020). doi:10.1142/S0129183120501545.

[40] M.J. Klein: Principle of Detailed Balance. Phys. Rev. **97** 1446–1447 (1955). doi:10.1103/PhysRev.97.1446.

[41] N. Kidambi, R.L. Harne, Y. Fujii, G.M. Pietron, K.W. Wang: Methods in Vehicle Mass and Road Grade Estimation. SAE Int. J. Passeng. Cars - Mech. Syst. **7** 2014-01–0111 (2014). doi:10.4271/2014-01-0111.

[42] US-EPA, Greenhouse Gas Inventory Guidance. Direct Emissions from Mobile Combustion Sources, US EPA Center for Corporate Climate Leadership (2016).

[43] N. Eissfeldt, R. Schrader: Calculation of street traffic emissions with a queuing model. Comput. Technol. **7** 5-15 (2002).

[44] A. Salcido, S. Carreón-Sierra: Air Pollutant Emissions in the Fukui-Ishibashi and Nagel-Schreckenberg Traffic Cellular Automata. J. Appl. Math. Phys. **05** 2140-2161 (2017). `doi:10.4236/jamp.2017.511175`.

[45] A. Ilachinski: Cellular Automata. A Discrete Universe. WORLD SCIENTIFIC (2001). `doi:10.1142/4702`.

[46] F. Bagnoli: Cellular Automata. In: Nonlinear Workbook. WORLD SCIENTIFIC. 257–274 (2011). `doi:10.1142/9789814335799_0010`.

[47] M. Cremer, J. Ludwig: A fast simulation model for traffic flow on the basis of boolean operations. Math. Comput. Simul. **28** 297–303 (1986). `doi:10.1016/0378-4754(86)90051-0`.

[48] M. Sasvári, J. Kertész: Cellular automata models of single-lane traffic. Phys. Rev. E. **56** 4104–4110 (1997). `doi:10.1103/PhysRevE.56.4104`.

[49] C.-J. Fu, B.-H. Wang, C.-Y. Yin, T. Zhou, B. Hu, K. Gao, P.M. Hui, C.-K. Hu: Analytical studies on a modified Nagel–Schreckenberg model with the Fukui–Ishibashi acceleration rule. Chaos, Solitons & Fractals. **31** 772–776 (2007). `doi:10.1016/j.chaos.2005.10.062`.

[50] N. Treiber, A. Kesting, C. Thiemann: How much does traffic congestion increase fuel consumption and emissions? Applying a fuel consumption model to the NGSIM trajectory data. In: Transportation Research Board 87th Annual Meeting, 17 (2008).

[51] M. Nyhan, S. Sobolevsky, C. Kang, P. Robinson, A. Corti, M. Szell, D. Streets, Z. Lu, R. Britter, S.R.H. Barrett, C. Ratti: Predicting vehicular emissions in high spatial resolution using pervasively measured transportation data and microscopic emissions model. Atmos. Environ. **140** 352–363 (2016). `doi:10.1016/j.atmosenv.2016.06.018`.

[52] W. Pan, Y. Xue, H.-D. He, W.-Z. Lu: Impacts of traffic congestion on fuel rate, dissipation and particle emission in a single lane based on Nasch Model. Phys. A Stat. Mech. Its Appl. **503** 154–162 (2018). `doi:10.1016/j.physa.2018.02.199`.

[53] V. Astarita, V.P. Giofrè, G. Guido, A. Vitale: A Single Intersection Cooperative-Competitive Paradigm in Real Time Traffic Signal Settings Based on Floating Car Data. Energies. **12** 409 (2019). `doi:10.3390/en12030409`.

[54] A. Madani, N. Moussa: Simulation of fuel consumption and engine pollutant in cellular automaton. J. Theor. Appl. Inf. Technol. **35** 250–257 (2012).

[55] X. Wang, Y. Xue, B. Cen, P. Zhang, H. He: Study on pollutant emissions of mixed traffic flow in cellular automaton. Phys. A Stat. Mech. Its Appl. **537** 122686 (2020). `doi:10.1016/j.physa.2019.122686`.

[56] D. Chu, Z. Deng, Y. He, C. Wu, C. Sun, Z. Lu: Curve speed model for driver assistance based on driving style classification. IET Intell. Trans. Syst. **11**, 501–510 (2017). `doi:10.1049/iet-its.2016.0294`